ELSEVIER

Applied Acoustics 62 (2001) 1229–1248

applied acoustics

www.elsevier.com/locate/apacoust

3D sound scattering by rigid barriers in the vicinity of tall buildings

L. Godinho, J. António, A. Tadeu *

Department of Civil Engineering, University of Coimbra, 3030-290 Coimbra, Portugal

Received 14 July 2000; received in revised form 3 January 2001; accepted 17 January 2001

Abstract

The boundary element method (BEM) is used to evaluate the acoustic scattering of a three-dimensional (3D) sound source by an infinitely long rigid barrier in the vicinity of tall buildings. The barrier is assumed to be non-absorbing and the buildings are modeled as an infinite barrier. The calculations are performed in the frequency domain and time signatures are obtained by means of inverse Fourier transforms. The 3D solution is obtained by means of Fourier transform in the direction in which the geometry does not vary. This requires solving a series of 2D problems with different spatial wavenumbers, k_z. The wavenumber transform in discrete form is obtained by considering an infinite number of virtual point sources equally spaced along the z axis. Complex frequencies are used to minimize the influence of these neighboring fictitious sources. Different geometric models, with barriers of varying sizes, are used. The reduction of sound pressure in the vicinity of the buildings is evaluated and the creation of shadow zones by the barriers is analyzed and compared with results provided by a simplified method.

Keywords: Acoustic barriers; Boundary element method; 3D source; 2-1/2D geometry

1. Introduction

One of the solutions most widely adopted by engineers for tackling the problem of noise generated by road traffic is the use of acoustic barriers. Many researchers are currently looking for ways to predict their efficiency correctly. Empirical methods are often used to solve practical engineering problems, but they fail to give accurate

* Corresponding author. Tel.: +351-239-797-201; fax: +351-239-797-190.
E-mail address: tadeu@dec.uc.pt (A. Tadeu).

0003-682X/01/$ - see front matter
PII: S0003-682X(01)00004-4

scientific solutions for sound propagation near the barrier. Various numerical methods have been developed to study this problem.

Many authors have used diffraction-based methods to analyze sound propagation in the presence of obstacles. Lam [1] introduced one such method for the calculation of the acoustic energy loss produced by the insertion of simple, finite length, three-dimensional (3D) acoustic barriers. Muradali and Fyfe [2] later extended this work to include the modeling of two-dimensional (2D) geometries. This work compares 2D and 3D models that take the presence of parallel barriers into account. Both coherent and incoherent line-sources are simulated.

Engineering practice employs several simplified models to compute the insertion loss of acoustic barriers (Beranek and Vèr [3], Barry and Reagan [4,5], Hanson et al [6]), estimating the attenuation by considering the diffraction effect on the edge of the barrier, in a simplified form.

Accuracy can be improved by using numerical methods like the boundary element method (BEM) or the finite element method to solve the wave-equation for each frequency to be considered. The major drawback of these methods is that they are very computer intensive, and are thus difficult to apply to very high frequencies. Using the theory of slender bodies, Filippi and Dumery [7] and Terai [8] developed a boundary integral equation technique to analyze the scattering of sound waves by thin rigid screens in unbounded regions. This method was subsequently extended by Kawai and Terai [9] to allow the prediction of sound attenuation by rigid barriers over a totally reflective ground surface. Duhamel [10] presented a numerical method which was based on the boundary elements method. This made it possible to calculate the 3D sound pressure around an acoustic barrier of constant but arbitrary cross-section placed over a rigid ground, making use of a set of simpler 2D solutions. Duhamel and Sergent [11] subsequently extended this work to accommodate absorption in the ground, and to compare numerical results obtained with experimental data. The influence of the shape and absorbent surface of railway noise barriers was assessed by Morgan, Hothersall and Chandler-Wilde [12], using a 2D boundary element model. Their work compares a boundary element prediction for simple barrier and vehicle shapes with results given by the standard UK prediction method in the case of railway noise barriers. Lacerda et al. [13] proposed a dual boundary element formulation for analyzing the 2D sound propagation around acoustic barriers, over an infinite plane, in which both the ground and the barrier were considered to be absorptive. The 3D propagation of sound around an absorptive barrier has been studied by Lacerda et al. [14], introducing a dual boundary element formulation that allowed the barrier to be modeled as a simple surface. This method avoided the problems caused by near-singular integrals and near-degenerate equation systems. The Green's function considered by the authors also took the properties of the ground into account, enabling absorptive ground to be modeled. More recently, Jean, Defrance and Gabillet [15] computed the efficiency of noise barriers in attenuating traffic noise, considering different source types such as point sources, coherent and incoherent line sources. They used a 2D boundary element method and obtained 3D responses by means of a post treatment of the 2D results. In this model, both the acoustic barrier and the ground surface are assumed to have absorbing properties.

The BEM is possibly the tool best suited to analyze wave propagation in unbounded media, because it automatically satisfies the far field radiation conditions. In addition, it allows a compact description of the medium in terms of boundary elements at the material discontinuities. Although the BEM leads to a fully populated system of equations, as opposed to the sparse system given by the finite difference and finite element techniques, the technique is efficient because the system matrix size is reduced.

This work takes into account both the influence of the acoustic barrier and the presence of very large buildings next to it. The pressure field generated by wave scattering at both objects is calculated using a standard boundary element formulation. Both the acoustic barrier and the building are assumed to be totally reflective. The Green's function used by the authors takes the presence of the tall building into consideration by using the images' method to simulate its presence, and therefore only interior boundaries need to be discretized by boundary elements.

In our model, the acoustic barrier is assumed to be of infinite length, while the acoustic source takes the form of a point load. This situation is usually referred to as a two-and-a-half-dimensional problem, for which solutions can be obtained by means of a spatial Fourier transform in the direction in which the geometry does not vary (Duhamel [10], Tadeu and Godinho [16]). This Fourier transformation in discrete form is obtained by considering an infinite number of virtual point sources equally spaced along the z axis, and sufficiently distant from one another to avoid spatial contamination of the response (Bouchon and Aki [17]). All the analyses are performed using complex frequencies, shifting down the frequency axis, in the complex plane. With this procedure, one can remove the singularities on (or near) the axis and minimize the influence of the neighboring fictitious sources (Phinney [18]). The 3D field in the time domain is then obtained by applying an inverse Fourier transform to the calculated response.

The present paper is organized as follows: first, the 3D acoustic problem is defined; then the BEM is formulated in the frequency domain, assuming the existence of a harmonic (steady state) line load whose amplitude varies sinusoidally in the third dimension. A brief validation of the BEM formulation is presented using a circular cylindrical rigid cavity placed inside an unbounded acoustic medium. The BEM model is then used to compute the 3D pressure field generated by a point pressure source in the vicinity of a rigid barrier placed between a source and a tall building, which is treated as an infinite rigid vertical plane surface. Simulation analyses are performed to investigate wave propagation in the vicinity of such buildings in the presence of neighboring acoustic barriers of varying sizes. Both frequency and time domain responses are obtained to permit a quantitative study of the 3D effects of the scattering. Finally, the results provided by the BEM model are compared with those computed using a simplified model that is currently in use.

2. Problem definition

The pressure field generated by a harmonic point load in a spatially uniform fluid medium is governed by

$$P_{\text{inc}} = \frac{A e^{\frac{i\omega}{\alpha}\left(\alpha t - \sqrt{(x-x_0)^2+y^2+z^2}\right)}}{\sqrt{(x-x_0)^2+y^2+z^2}} \tag{1}$$

in which ω is the oscillating frequency, $(x_0, 0, 0)$ is the position of the load, the subscript *inc* denotes the incident field, A is the wave amplitude, α is the pressure wave velocity of the medium, and $i = \sqrt{-1}$.

Fourier-transforming Eq. (1) in the z direction, and using the effective wavenumbers, $k_\alpha = \sqrt{\frac{\omega^2}{\alpha^2} - k_z^2}$ with $Imk_\alpha < 0$, where k_z is the axial wavenumber, we obtain

$$\hat{p}_{\text{inc}}(\omega, x, y, k_z) = \frac{-iA}{2} H_0^{(2)}\left(k_\alpha \sqrt{(x-x_0)^2+y^2}\right) \tag{2}$$

in which the $H_n^{(2)}(...)$ are second Hankel functions of order n.

If one assumes the existence of an infinite set of evenly-spaced sources along the z direction, the former incident field may be written as

$$p_{\text{inc}}(\omega, x, y, z) = \frac{2\pi}{L} \sum_{m=-\infty}^{\infty} \hat{p}_{\text{inc}}(\omega, x, y, k_z) e^{-ik_z z} \tag{3}$$

where L is the spatial source interval, and $k_z = \frac{2\pi}{L} m$. Thus, the 3D pressure field may be obtained as the pressure irradiated by a sum of harmonic (steady-state) line loads whose amplitude varies sinusoidally in the third dimension. This sum converges and can be approximated by a finite number of terms.

The problem to be solved concerns a spatially uniform acoustic medium bounded by two perpendicular flat surfaces: one simulates the horizontal flat surface, while the other models the tall building. A vertical rectangular rigid obstacle (acoustic barrier) is placed inside this medium. The pressure field defined by Eq. (3) needs to be reformulated to satisfy the boundary conditions: null normal velocities at both the horizontal flat surface and the rigid infinite vertical wall. These conditions can be satisfied automatically by superposing the pressure field generated by the real source plus three virtual sources (image sources), located in such a way that they constitute mirrors in relation to the vertical and horizontal planes. The pressure field [Green's function $G(x, x_0, \omega)$] can then be computed by the following expression, when the vertical plane and the horizontal plane are defined by $x = 0$ and $y = 0$, respectively:

$$G(x, x_0, \omega) = \sum_{j=1}^{NS} \frac{-i}{4} \left[H_0(k_\alpha r_j)\right] \tag{4}$$

in which $NS = 4$,

$$r_1 = \sqrt{(x - x_0)^2 + (y - y_0)^2}$$

$$r_2 = \sqrt{(x - x_0)^2 + (y + y_0)^2}$$

$$r_3 = \sqrt{(x + x_0)^2 + (y - y_0)^2}$$

$$r_4 = \sqrt{(x + x_0)^2 + (y + y_0)^2}$$

3. Boundary element formulation

A standard BEM formulation is used to calculate the three-dimensional scattering field generated by a rigid, vertical, rectangular, two-dimensional obstacle placed inside an acoustic medium and illuminated by a pressure point load. As described above, the resulting 2−1/2−D problem can be solved as a discrete summation of the 2D BEM solutions for different k_z wavenumbers. In order to perform the wavenumber transform in discrete form, an infinite number of virtual point sources, equally spaced along the z axis, is considered. The spacing between the virtual sources is sufficiently large to prevent the spatial contamination of the response (Bouchon and Aki [17]). The 3D field can then be obtained using the inverse spatial Fourier transform.

Given the extensive literature available, the details of the BEM formulation required for the type of the scattering problem presented here are omitted (see, for example, Manolis and Beskos [19]). It is nevertheless important to state that each two-dimensional problem requires the evaluation of the integral

$$H^{kl} = \int_{C_l} H(\underline{x}_k, \underline{x}_l, n_l) dC_l \tag{5}$$

in which H^{kl} is the pressure velocity component at $\underline{x}_k$ due to pressure load at $\underline{x}_l$ and n_l is the unit outward normal for the lth boundary segment C_l. The required pressure velocity function is obtained by differentiating Eq. (4) in relation to the unit outward normal.

Application of Eq. (5) to a set of boundary elements used to discretize the boundary of the acoustic barrier leads to a system of equations that relates the pressure field to a set of nodal pressure values. The nodal pressure values are calculated after this system of equations has been mathematically manipulated and null velocity along the outward normal direction of the boundary elements imposed. The

required integrations in Eq. (5) are performed with Gauss–Legendre quadrature, using six integration points. Since the acoustic barrier is modeled as a thick object, numerical integrations on elements close to or directly facing each other are performed using a higher order Gauss–Legendre quadrature.

The scattered pressure field at any point inside the acoustic medium can then be calculated in relation to the nodal pressure values calculated previously:

$$p^k_{\mathrm{sca}} = \sum_{l=1}^{N} p^l H^{kl} \tag{6}$$

In this equation, p^k_{sca} is the scattered pressure field at receiver k, N is the total number of boundary elements, and p^l is the nodal pressure value at element l.

4. Pressure in time-space

Responses in the time domain are calculated by means of an inverse fast Fourier transformation in ω, using an acoustic source, with temporal variation given by a Ricker pulse. Since it decays rapidly in both the time and frequency domains, this type of pulse allows a convenient reduction in the computational effort and an easier interpretation of the time signatures. The Ricker function can be expressed by:

$$u(\tau) = A(1 - 2\tau^2)\mathrm{e}^{-\tau^2} \tag{7}$$

in which A is the amplitude, $\tau = (t - t_s)/t_0$ and t represents the time, with t_s being the time when the maximum occurs, while πt_0 is the dominant wavelet period. By applying a Fourier transformation to this function, one obtains:

$$U(\omega) = A\left[2\sqrt{\pi t_0} e^{-i\omega t_s}\right]\Omega^2 \mathrm{e}^{-\Omega^2} \tag{8}$$

where $\Omega = \omega t_0/2$.

The Fourier transformations required are achieved by adding together a finite number of terms, expressed as either frequencies or wavenumbers. This is equivalent to adding periodic sources at spatial intervals of $L = 2\pi/\Delta k_z$ and temporal intervals of $T = 2\pi/\Delta\omega$. In these expressions, Δk_z and $\Delta\omega$ represent the wavenumber and frequency increments, respectively. To prevent the contamination of the response by the periodic sources, the spacing between them must be large enough to ensure that their contribution arrives at times later than T. This is achieved by shifting the frequency axis slightly downwards in the complex plane, using complex frequencies with an imaginary part of the form $\omega_c = \omega - i\eta$ (with $\eta = 0.7\Delta\omega$). With this technique, the contribution of the virtual sources is considerably diminished. When the

response is calculated in the time domain, this change must be taken into account by rescaling the response, applying an exponential window $e^{\eta t}$, Kausel [20].

5. Validation of the BEM algorithm

The BEM algorithm is validated by taking a cylindrical circular rigid pipe placed inside an unbounded homogeneous acoustic medium ($\alpha = 340$m/s), illuminated by a harmonic point pressure load applied at point O (Fig. 1), for which the solution is known in closed form. The required Green's function is obtained by setting the NS parameter in Eq. (4) to 1.

The response is calculated for a single receiver placed at $x = 6.0$ m and $y = -6.0$ m, for frequencies ranging from 4 to 512 Hz, taking a constant value for $k_z = 1.0$rad/m. Fig. 2 displays the real and imaginary parts of the response for the analytical solution and the numerical BEM error when 25 constant boundary elements were used to model the inclusion, calculated as the amplitude of the difference between both solutions. Analysis of the results shows that the BEM approach for low frequencies is extremely accurate, and reveals only slight differences at high frequencies. This behaviour is due to the fact that the BEM performance improves with the ratio of the wavelength of the incident waves to the length of the boundary elements. In our example, this ratio decreases from 298 (4 Hz) to 3 (512 Hz).

6. Numerical examples

The method described above was used to study the influence of an acoustic barrier placed between a point pressure load and a very tall building. In our examples, both the ground surface and the building were considered to be non-absorbing, while the

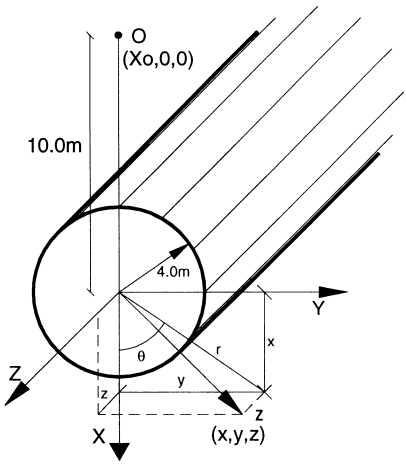

Fig. 1. Geometry of the problem.

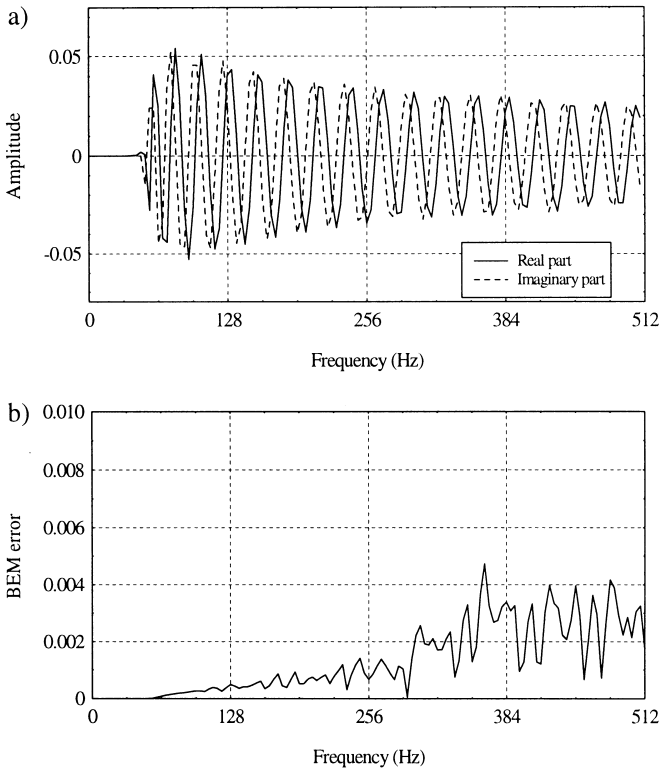

Fig. 2. Validation results: (a) analytical solution; (b) BEM error.

host acoustic medium had a pressure wave velocity of 340 m/s. A point acoustic source is placed 0.6 m above the ground and 25.0 m from the tall building. An acoustic barrier of height h is placed in front of the building (with its plane of symmetry at $x = 20.0$m), to reduce the sound level registered on its façade (Fig. 3).

The acoustic barrier is modeled as a body 0.2 m thick, and it is discretized using an appropriate number of boundary elements, defined by the relation between the wavelength and the length of the boundary elements, which was set at 8. The number of boundary elements used is never less than 32. To ensure accuracy, the required numerical integrations [Eq. (6)] are performed using a Gauss–Legendre quadrature integration scheme, where the number of sampling points increases as the distance between the loaded element and the element to be integrated decreases. To check that the correct number was being used, the performance of the solution was tested using a very high number of integration points.

The rest of this section is divided into two parts. In the first part, the scattering produced by a rigid barrier is analysed according to the results calculated using the BEM. Simulation analyses are performed in the frequency and time domains, identifying the attenuation provided by the acoustic barrier. In the second part, these results are compared with those provided by a simplified model.

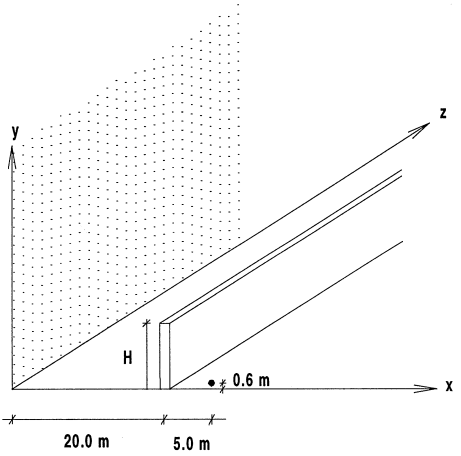

Fig. 3. Geometry of the problem.

6.1. Scattering by rigid barriers via the BEM

The response was first evaluated over a vertical grid of receivers placed at $z = 0.0$m, for excitation frequencies of 125.0 and 1000.0 Hz. Calculations were performed in the absence of acoustic barriers, and in the presence of barriers 2.0, 4.0 and 6.0 m high. Fig. 4 presents the sound pressure level calculated by the expression $10\log\left[p^2/\left(2\times10^{-5}\right)^2\right]$, where p refers to the pressure amplitude and 2×10^{-5} is the pressure of reference. These plots use a gray scale, ranging from white to black as the amplitude increases.

In the absence of an acoustic barrier (Fig. 4a), the pressure field results from the direct incident field interacting with that reflected by the ground surface and the building. Thus, the total field is given by the sum of waves with different phases leading to a spatially variable sound pressure level, distinguishable in Fig. 4 as a pattern of differently colored zones. This phenomenon becomes more complex as the frequency increases.

Fig. 4b–d illustrate the sound pressure level when a barrier is inserted. Analysis of the results shows the existence of a "shadow" zone, behind the barrier, where a pronounced attenuation of the sound pressure field is registered. This "shadow" becomes more intense as the height of the barrier changes, increasing from 2.0 to 4.0 m and then to 6.0 m, at the same time as the frequency increases from 125.0 to 1000.0 Hz. This phenomenon was expected since the diffracted field increases as the ratio between the wavelength of the incident field and the size of the illuminated object decreases. Notice that this happens when the height of the barrier and the excitation frequency both increase. A bigger "shadow" behind the barrier is associated with an enhanced wave field being reflected back to the highway. It can further be observed that the attenuation created by the barrier, provided by the "shadow" effect, decreases as the distance of the receivers from the ground surface

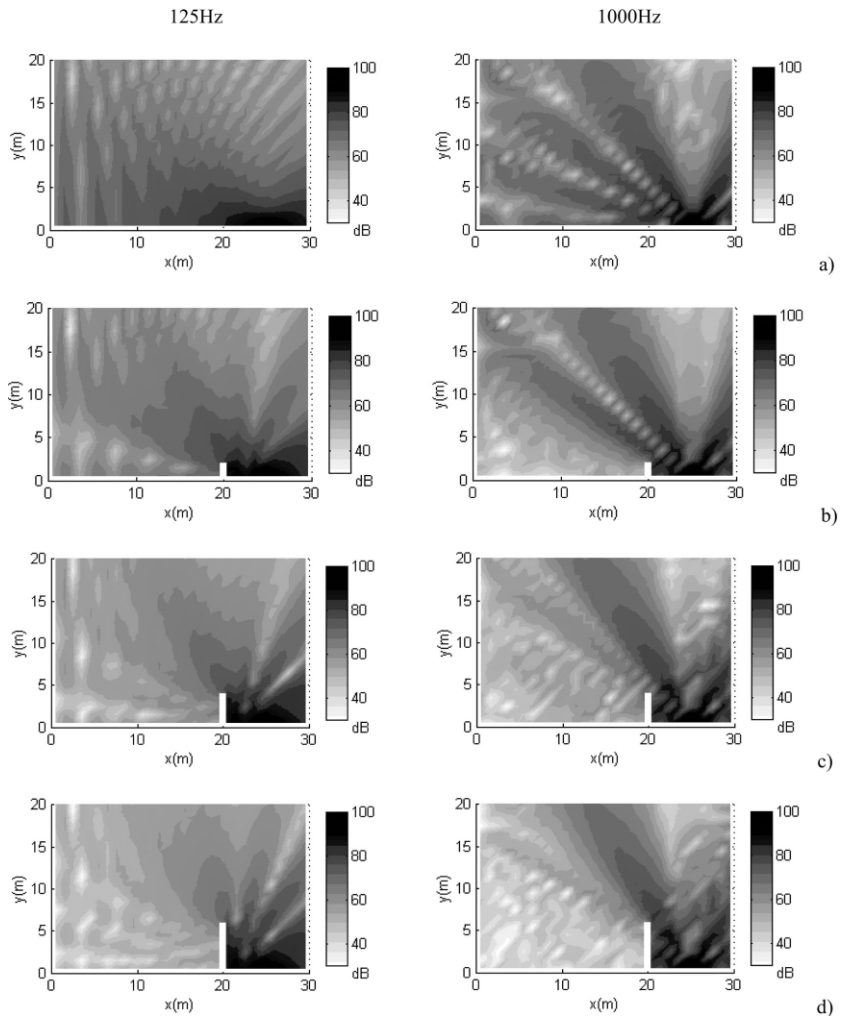

Fig. 4. Sound pressure level along an xy plane at $z=0$ for differently sized barriers: (a) $h=0.0$ m; (b) $h=2.0$ m; (c) $h=4.0$ m; (d) h = 6.0 m.

grows. It is also interesting to note the existence of a wave field created by diffraction at the edge of the barrier, as revealed by the wave field patterns radiating from it.

The "shadow" effect behind the barrier is still detected at receivers placed further away from the plane of the source, $z \neq 0$ (not illustrated). As the distance of the receivers along the z direction increases, the sound pressure field becomes more uniform. At very large distances, the resulting field can even be treated as a plane wave.

To better illustrate the propagation of the sound pressure from its source to the receivers, the time responses are presented for a barrier 4.0 m tall. At time $t = 0.0$ ms a spherical pulse is emitted from a point pressure source located at $x = 25.0$ m, $y = 0.6$ m and $z = 0.0$ m. The calculations were performed for frequencies ranging from

2.5 to 320.0 Hz, with a frequency increment of 2.5 Hz, determining a total time frame of 0.4 s. The amplitude of the source, A, in Eqs. (1) and (2) is set to the unit. The source time dependence is assumed to be a Ricker wavelet, and time responses were calculated for characteristic frequencies of 63 and 125 Hz.

In Fig. 5 a sequence of snapshots displays the pressure wave field along a grid of receivers placed at $z = 0.0$m. In these figures, the pressure amplitude is represented by a gray scale ranging from white to black, as the amplitude increases.

As the pulse propagates away from the source, the wave energy spreads out. At time $t = 14.4$ ms the spherical incident pulse reaches the acoustic barrier, where it is scattered by reflection, traveling back to the highway. As the time progresses the incident pulse strikes the edges of the barrier, where it is diffracted, generating a pulse that propagates in all directions, even along the vertical faces of the barrier.

The first plot, at $t = 31.3$ ms (Fig. 5a), records the wave field generated when the incident pulse has passed the acoustic barrier, and the diffracted pulses have already reached the ground surface, where they are reflected. The "shadow" created behind the barrier is well-defined, increasing as the characteristic frequency of the source changes from 63 to 125 Hz.

At $t = 47.7$ ms the incident pulse is further away from its origin (Fig. 5b). The former diffracted pulse, travelling along the barrier, is already well developed, moving

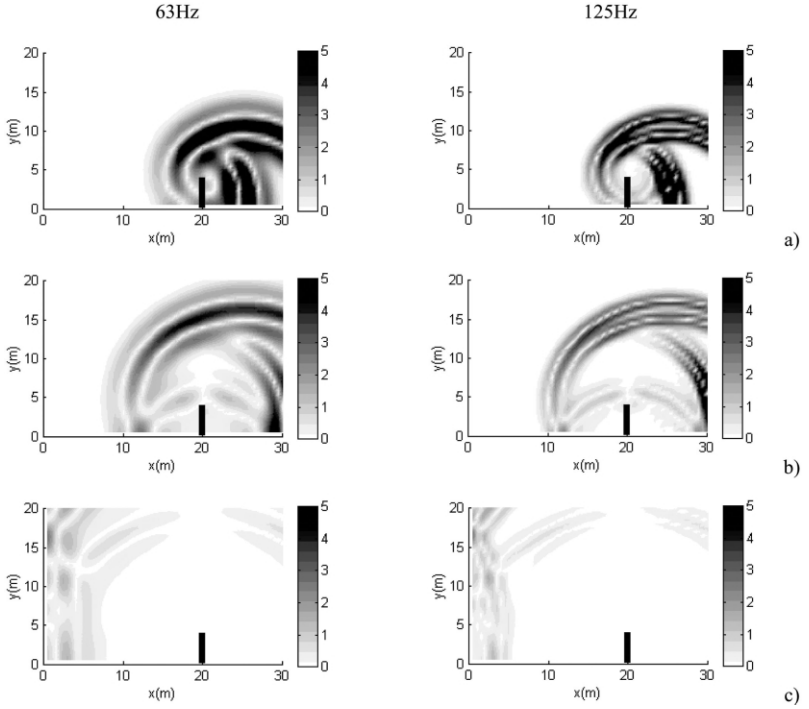

Fig. 5. Time response over a vertical grid of receivers, placed perpendicularly to the building at $z = 0.0$ m, for a barrier of $h = 4.0$ m. (a) $t = 31.3$ ms; (b) $t = 47.7$ ms; (c) $t = 88.3$ ms.

away from the barrier, after being reflected by the ground surface. The interaction of the direct pulses diffracted from the edge of the barrier with those first reflected by the ground, gives rise to an enhanced wave pulse that travels along the ground surface.

As time elapses, the wavefront hits the building, where is reflected, traveling back as illustrated in the snapshot at $t = 88.3$ ms (Fig. 5c). Later, part of these reflected pulses strikes the rigid surface of the barrier again, and remains trapped between the barrier and the building.

Fig. 6 presents the pressure wavefield when the above grid of receivers is positioned at $z = 30.0$ m. Fig. 6a registers the arrival of the first pulses at this plane of receivers ($t = 88.3$ ms). The amplitude of the wave field at receivers placed before the barrier ($x > 20.1$ m) shows a high concentration of energy as the result of the almost simultaneous arrival of the incident pulse and the different reflected pulses on the barrier and ground surface. For larger z distances the wave field produced can even be seen as a plane incident wave.

At $t = 100.8$ ms (Fig. 6b) the "shadow" effect produced by the presence of the barrier is easily visible. The effect of the interaction of the direct pulses diffracted from the edge of the barrier with those first reflected at the ground surface can now be observed as a significant effect over a larger spatial domain at receivers placed closer to the ground surface. This effect decreases as the frequency increases from 63 to 125 Hz.

The response was then evaluated at a grid of receivers placed along a vertical plane 0.5 m away from the rigid wall, and equally spaced at 1.0 and 4.0 m apart along the vertical and longitudinal directions, respectively. The source time dependence is assumed to be a Ricker wavelet with a characteristic frequency of 125 Hz.

Fig. 7 presents the sound pressure level computed by the expression $10 \log \left[p^2/\left(2\times10^{-5}\right)^2\right]$, where p refers to the maximum amplitude of the time responses

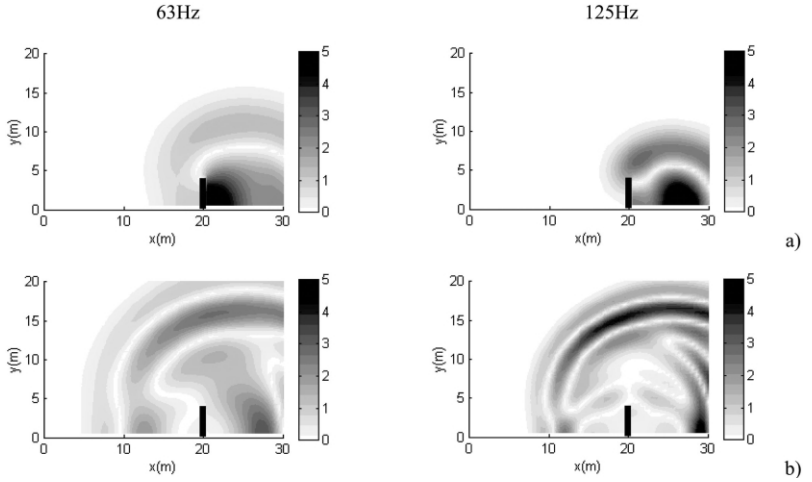

Fig. 6. Time response over a vertical grid of receivers, placed perpendicularly to the building at $z = 30.0$ m, for a barrier of $h = 4.0$ m. (a) $t = 88.3$ ms; (b) $t = 100.8$ ms.

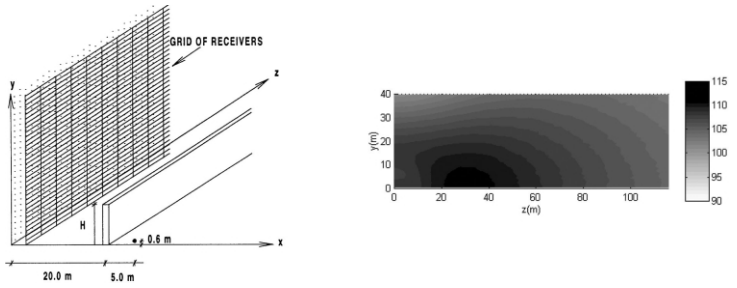

Fig. 7. Sound pressure level along a vertical plane 0.5 m away from the building.

calculated for each receiver, ascribing $A = 1$ in Eqs. (1) and (2), obtained when there is no barrier. The results show that the maximum sound pressure level field is not obtained at $z = 0.0$ m. The interaction of the directly incident pulses with those reflected by the building explains this behaviour, which does not occur if the grid of receivers is moved to $x = 0.0$ m (not illustrated). A general reduction in the sound pressure level is noted as the distance between the receiver and the source increases.

Fig. 8 displays the sound pressure level, calculated as described above, and its attenuation when a barrier is inserted between the source and the building. The results obtained for a barrier 2.0 m tall indicate that the barrier performs less well for receivers placed closer to the ground, owing to the interaction of the direct field diffracted by the barrier with that reflected by the ground surface. The characteristic frequency of the pulse of 125 Hz defines a wavelet with sufficient length to promote

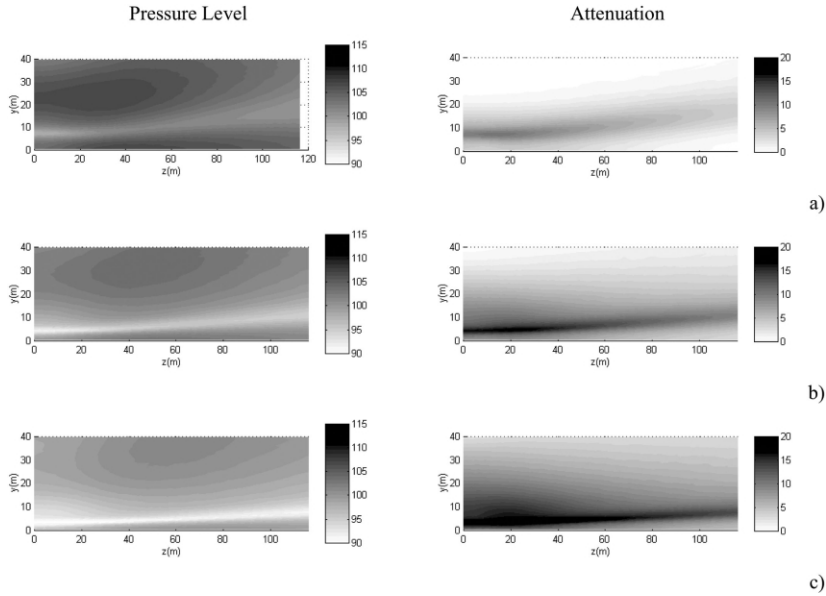

Fig. 8. Sound pressure level and attenuation along a vertical plane 0.5 m away from the building, for barriers (a) 2, (b) 4 and (c) 6 m tall.

the interference between these waves for receivers placed closer to the ground surface. The performance of the barrier improves as receivers are placed further away from the ground surface, reaching maximum efficiency at approximately 8 m above the ground for $z = 0.0$ m. Above this value the barrier loses efficiency, even being outperformed by the case where there is no barrier, at greater distances from the ground. The performance of the acoustic barrier is not constant along the z axis. A line following the points of maximum efficiency, for consecutive vertical z planes, is inclined, indicating better performances at receivers placed further above the ground surface as z increases. It appears that the reflections from the ground close to the building, mentioned above, become more important as z increases, as the time responses show.

As the height of the barrier increases from 2.0, to 4.0 m and then to 6.0 m, the sound pressure level attenuation increases for the full domain of receivers. The above-defined line of maximum efficiency is closer to the ground surface and less inclined. It seems that the waves reflected from the ground close to the building and the direct field diffracted by the barrier lose importance relative to the receivers closer to the ground surface as the barrier increases in height.

6.2. Barrier insertion loss via the BEM vs. simplified models

Several simplified models are currently used to estimate the insertion loss of acoustic barriers. One such method (Beranek and Vèr [3], Barry and Reagan [4], Hanson et al. [5]) considers that this attenuation can be estimated by taking into account the diffraction effect on the edge of the barrier. If the barrier is considered to be thin and infinitely long, and the acoustic waves are emitted by a point source, this attenuation can be calculated by

$$\begin{cases} 20\log\dfrac{\sqrt{2}\pi N}{\tan(\sqrt{2}\pi N)} + 5 \geqslant 0 \text{ outside shadow} \\ 20\log\dfrac{\sqrt{2}\pi N}{\tanh(\sqrt{2}\pi N)} + 5 \leqslant 20 \text{ inside shadow} \end{cases} \tag{9}$$

In these equations, N represents the Fresnel number given by $\frac{2(r-d)}{\lambda}$, where r is the length of the travel path for the diffracted acoustic ray, d is the length of the travel path for the incident ray when there is no obstacle, and λ is the wavelength in meters. Analysis of Eqs. (9) shows that the attenuation is bounded by an upper value of 20 dB.

This simplified model has been used to estimate the barrier attenuation at a grid of receivers placed along a vertical plane at $x = 0.0$ m, equally spaced 1.0 and 4.0 m apart along the vertical and longitudinal directions, respectively. This method can be applied to our specific scenario (a barrier in the vicinity of a tall building), because absorption is absent at the façade of the building, and the grid of receivers is coincident with the rigid wall ($x = 0.0$ m). Indeed, in our scenario the pressure level increases by 6 dB at $x = 0.0$ m, given the presence of the building, but the attenuation provided by

the acoustic barrier is still the same. Notice that the insertion loss is calculated here as the difference between the pressure levels, $10\log\left[p^2/\left(2\times10^{-5}\right)^2\right]$, where p is the maximum amplitude of the time responses calculated for each receiver, obtained with and without the acoustic barrier. Thus, the later pulses arriving at the grid of receivers, originated by the multiple reverberations between the rigid wall and the barrier, do not contribute to the final value for the insertion loss, as they have a pronounced amplitude decay.

The barrier insertion loss has been calculated using both the BEM and the simplified method presented above, for barriers 2, 4 and 6 m tall. Figs. 9 and 10 give the individual insertion losses and their difference, calculated by both the BEM and the simplified model for excitation frequencies of 63 and 125 Hz, respectively.

Fig. 9a illustrates the response when a barrier 2 m tall is inserted. Analysis of the results shows that the attenuation difference is low when the receivers are placed on a z plane at small distances from the source. As the distance increases, the attenuation for receivers placed in the vicinity of the ground surface, predicted by the simplified model, is markedly larger than that calculated by the BEM. The effect of the interaction of the direct field diffracted by the barrier with that reflected by the ground surface explains the observed worse performance of the barriers close to the ground. This factor is not taken into account when the calculations are performed by the simplified diffraction model. These features are even more evident for receivers placed further away along z, where the simplified model predicts higher attenuation levels closer to the ground than the BEM, for receivers placed further away from the ground surface. The BEM results indicate an improvement in the performance of the acoustic barrier for receivers placed above the spatial zone controlled by the reflections at the ground surface. As explained above, the y position of the receivers (distance from the ground surface), where the results are better, is not constant along the z axis, but tends to increase with a simultaneous decrease of attenuation. The simplified model only predicts an attenuation that decreases as both z and y increase.

As the height of the barrier changes from 2 to 4 m and then to 6 m, the BEM solution predicts an acoustic attenuation with a markedly better performance for those receivers placed at an intermediate distance from the ground surface. The negative effect of the reflections at the ground surface is further limited at smaller distances from the ground surface, as the height of the barrier increases. Very close to the ground, however, the performance of the barrier decreases even for taller barriers. The simplified model does not allow the results to improve as the distance of the receivers to the ground surface increases. Thus, the simplified models predict a better performance by the barrier at receivers placed closer to the ground, and does not accommodate a better performance of the barriers for receivers placed at intermediate distances from the ground surface, as envisaged by the BEM. This difference in behaviour is even more evident as the receivers are placed further away from the z plane of the source, where the BEM results show a steady drop in performance for receivers placed in the vicinity of the ground at greater distances from the ground, as z increases.

As the excitation frequency of the incident pulse increases to 125 Hz, the responses exhibit similar features (see Fig. 10). Calculations performed using the BEM model predict a poorer interaction of the direct field diffracted by the barrier with that

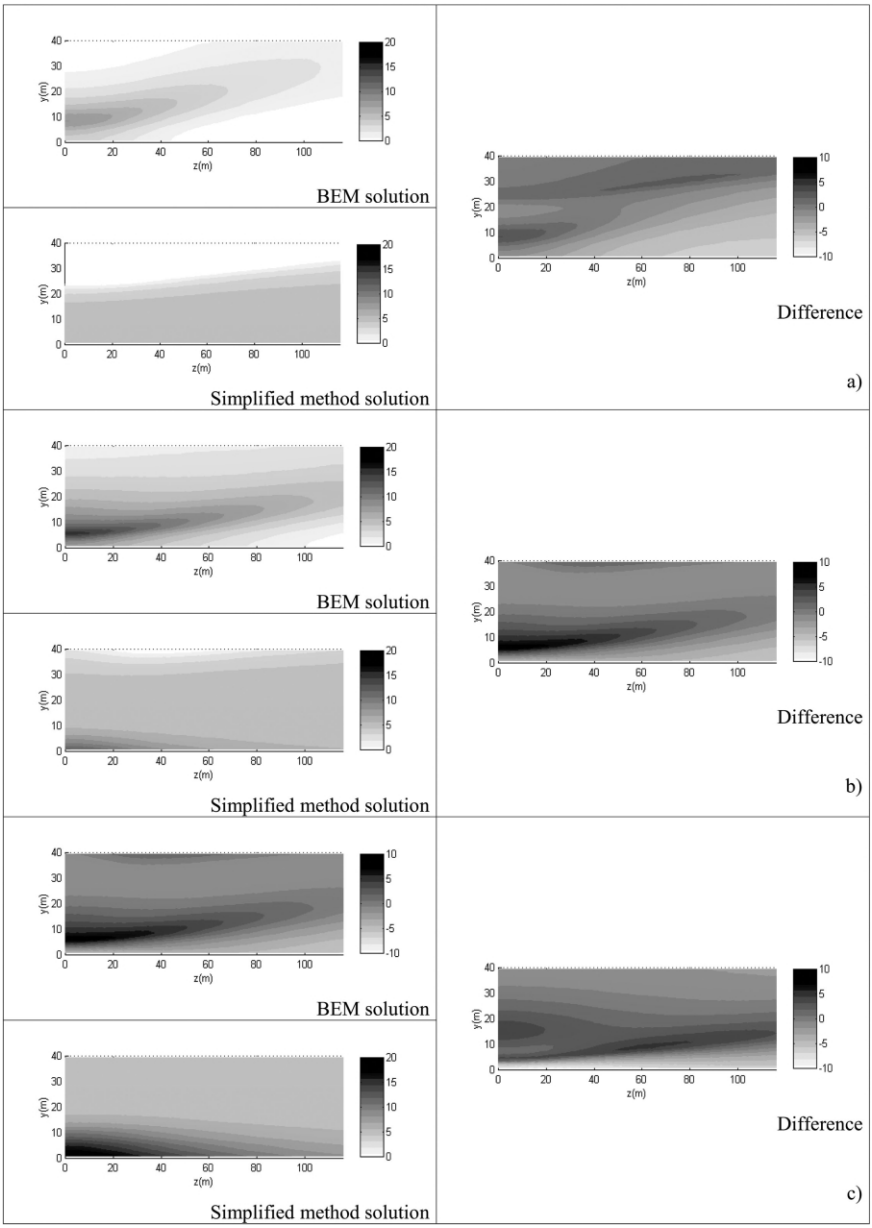

Fig. 9. Comparison between insertion losses calculated by the BEM and by a simplified model for a frequency of 63 HZ. (a) $h = 2.0$ m; (b) $h = 4.0$ m; (c) $h = 6.0$ m.

reflected by the ground surface, as shown by the bigger attenuation levels at receivers closer to the ground. The attenuation patterns for the simplified model are similar to the ones found for 63 Hz: it predicts a better performance by the barrier at

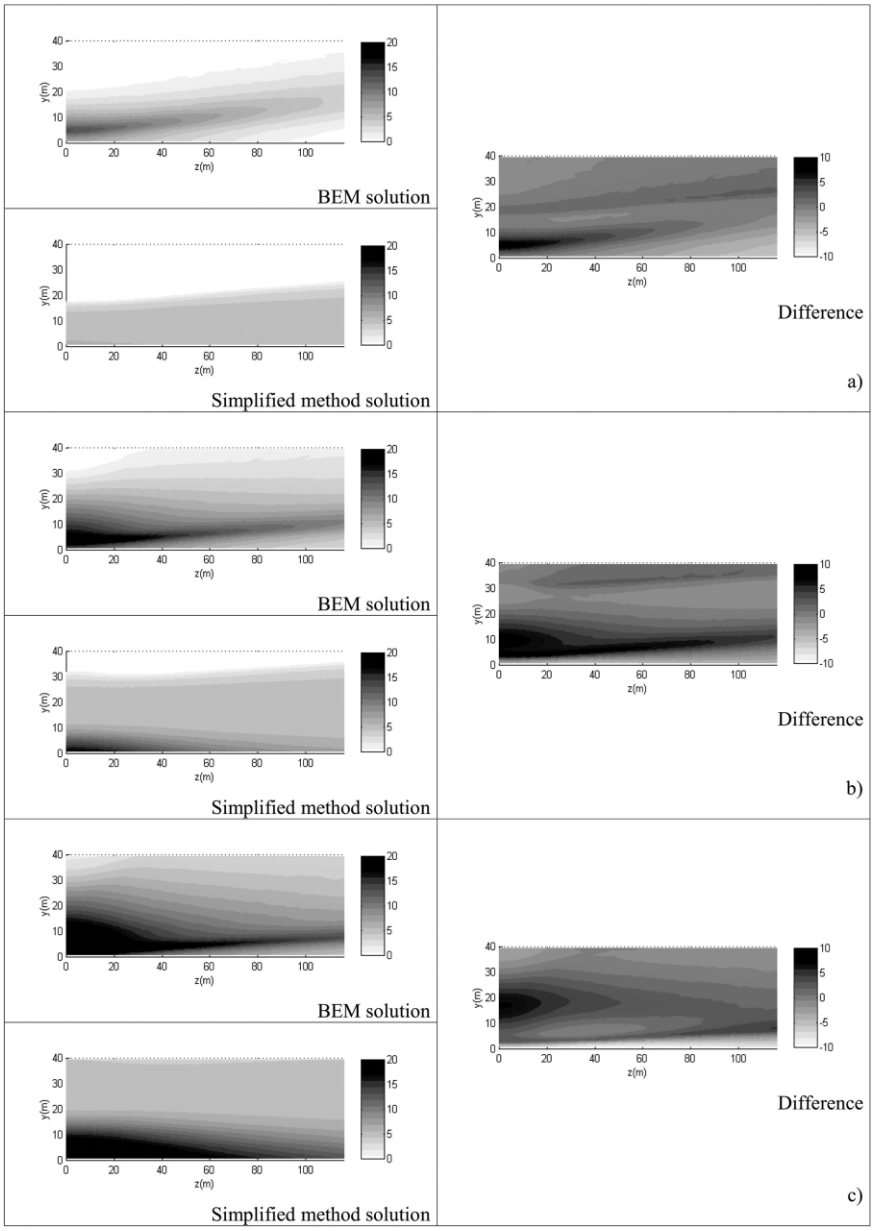

Fig. 10. Comparison between insertion losses calculated by the BEM and by a simplified model for a frequency of 125 Hz. (a) $h = 2.0$ m; (b) $h = 4.0$ m; (c) $h = 6.0$ m.

receivers closer to the ground than the BEM does, and does not allow a better performance of the barrier at receivers placed at some distance above the ground surface. It should be noted that, when the receivers are placed closer to the rigid ground

surface and the z distances are larger, the attenuation levels predicted by the simplified method can be 7 dB higher than those predicted by BEM.

In engineering practice, the type of noise source may differ from the simpler wavelet used here, a Ricker pulse. These sources would require calculation to be done over a different frequency domain. The BEM solutions would still be possible, but the computational cost for larger frequency domains would be higher. Nevertheless, the results described above would still be valid in relation to other types of source. For any source type, the importance of the reflected field at the ground, closer to a barrier (building), heralds a poorer performance by an acoustic barrier, not predicted by the simplified model used. The BEM results would have approached the simplified model solution if the ground surface had been modeled with high absorption properties.

7. Conclusions

The 2−1/2 BEM formulated was found to be suitable for studying the influence of an acoustic barrier placed between a point sound pressure load and a very tall building.

Results obtained in the frequency domain show that the performance of a low barrier is poorer at receivers placed closer to the ground surface when the frequency is low. For higher frequencies, the barrier creates a "shadow" zone behind it, leading to a pronounced attenuation of the sound pressure field at the lower receivers. The efficiency of the barrier improves further if its height increases, creating a more intense "shadow" zone behind it.

Analysis of the sound pressure level obtained over a plane of receivers placed parallel to the building indicates a non-uniform performance by the acoustic barrier. Receivers close to the ground show that the interaction between the direct field diffracted by the edge of the barrier with that first reflected on the ground leads to the barrier performing less well. Thus, improved behaviour is found at receivers placed at some distance from the ground. As z increases, the maximum efficiency is observed at receivers placed further away from the ground surface. As the barrier becomes taller the sound pressure level attenuation increases, for the full spatial domain of receivers, and a maximum efficiency is found at receivers placed closer to the ground.

Time–domain analysis was also performed to better understand the influence of the acoustic barrier on the propagation of a spherical pulse. This analysis confirmed that interaction occurred between pulses diffracted directly at the edge of the barrier and pulses first reflected on the rigid ground, generating an enhanced field in the direct vicinity of the ground.

Important differences between the BEM results and those provided by a simplified model emerged. The simplified model predicts higher attenuation levels at receivers in the close vicinity of the ground and does not indicate improved performance by the barrier at receivers placed further away from the ground surface. This is even true for receivers placed away from the z plane of the source. The simplified model

does not appear to take full account of the poorer performance of the acoustic barrier for receivers in the vicinity of the ground, as the BEM does. Furthermore, the BEM tends to predict higher attenuation values for receivers placed further from the ground. These differences are even more important as z increases, when the simplified model predicts higher attenuation levels close to the ground than the BEM does.

In spite of the general validity of the results presented here, it is important to bear in mind that they have been calculated assuming the existence of an homogeneous atmosphere and rigid surfaces, which may not match real outdoor conditions. Also, only lower frequency results, less than 1000 Hz, have been computed. Higher frequency responses that approach the upper bound of the domain of frequencies produced by traffic noise, would maintain the main features found in this work.

References

[1] Lam YW. Using Maekawa's chart to calculate finite length barrier insertion loss. Appl Acoust 1994;42:29–40.
[2] Muradali A, Fyfe KR. A study of 2D and 3D barrier insertion loss using improved diffraction-based methods. Appl Acoust 1998;53:49–75.
[3] Beranek LL, Vér IL. Noise and vibration control engineering, Wiley Interscience, 1992.
[4] Barry TM, Reagan JA. FHWA highway traffic noise prediction model. US federal highway administration. Report FHWA-RD-7-108, 1978, Washington, DC, USA.
[5] FHWA highway traffic noise model. US federal highway administration. Report FHWA-PD-96-010, 1998. Washington DC, USA.
[6] Hanson CE, Saurenman HJ, Anderson GS, Towers DA. Guidance manual for transit noise and vibration impact assessment. US urban mass transportation administration, Report UMTA-DC.08-9091-90-1, 1990. Washington DC, USA.
[7] Filippi P, Dumery G. Etude théorique et numérique de la diffraction par un écran mince. Acustica 1969;21:343–59.
[8] Terai T. On calculation of sound fields around three-dimensional objects by integral equation methods. J Sound Vib 1980;69:71–100.
[9] Kawai Y, Terai T. The application of integral equation methods to the calculation of sound attenuation by barriers. Appl Acoust 1990;31:101–17.
[10] Duhamel D. Efficient calculation of the three-dimensional sound pressure field around a noise barrier. J Sound Vib 1996;197(5):547–71.
[11] Duhamel D, Sergent P. Sound propagation over noise barriers with absorbing ground. J Sound Vib 1998;218(5):799–823.
[12] Morgan PA, Hothersall DC, Chandler-Wilde SN. Influence of shape and absorbing surface–a numerical study of railway barriers. J Sound Vib 1998;217(3):405–17.
[13] Lacerda LA, Wrobel LC, Mansur WJ. A dual boundary element formulation for sound propagation around barriers over an infinite plane. J Sound Vib 1997;202:235–347.
[14] Lacerda LA, Wrobel, LC, Power H, Mansur WJ. A novel boundary integral formulation for three-dimensional analysis of thin acoustic barriers over an impedance plane. J Acoust Soc Am 1998;104(2):671–8.
[15] Jean P, Defrance J, Gabillet Y. The importance of source type on the assessment of noise barriers. J Sound Vib 1999;226(2):201–16.
[16] Tadeu A, Godinho L. 3D wave scattering by a fixed cylindrical inclusion submerged in a fluid medium. Eng An Bound El 1999;23:745–56.
[17] Bouchon M, Aki K. Discrete wave-number representation of seismic source wavefields. Bull Seism Am 1977;67:259–77.

[18] Phinney RA. Theoretical calculation of the spectrum of first arrivals in layered elastic mediums. J Geophys Res 1965;70:5107–23.
[19] Manolis GD, Beskos DE. Boundary element methods in elastodynamics. London: Unwin Hyman Chapman and Hall, 1988.
[20] Kausel E. Forced vibrations of circular foundations in layered media. MIT Research Report 70–3. 1974. Department of Civil Engineering, MIT, Cambridge, USA.